^{5}He, ^{7}He, and ^{8}Li ($E^{*}=2.26$ MeV) intermediate ternary particles in the spontaneous fission of ^{252}Cf

Yu. N. Kopatch,[1,2,*] M. Mutterer,[1] D. Schwalm,[3] P. Thirolf,[3,†] and F. Gönnenwein[4]
[1]*Institut für Kernphysik, Technische Universität, D-64289 Darmstadt, Germany*
[2]*Frank Laboratory of Neutron Physics, JINR, RU-141980 Dubna, Russia*
[3]*Max-Planck-Institut für Kernphysik, D-69115 Heidelberg, Germany*
[4]*Physikalisches Institut der Universität Tübingen, D-72076 Tübingen, Germany*
(Received 10 December 2001; published 1 April 2002)

The neutron-unstable odd-N isotopes ^{5}He, ^{7}He, and ^{8}Li (in its excited state of $E^{*}=2.26$ MeV) were measured to show up as short-lived ($\tau\simeq10^{-21}-10^{-20}$ s) intermediate light charged particles (LCPs) in ternary fission of ^{252}Cf. For the study a high-efficiency angular correlation measurement between neutrons, LCPs, and main fission fragments has been performed. The evidence for the ternary ^{5}He and ^{7}He particles (lifetimes: 1×10^{-21} s, and 4×10^{-21} s, respectively) was disclosed from the measured angular distributions of their decay neutrons focused by the emission in flight towards the direction of motion of ^{4}He and ^{6}He ternary particles. Similarly, neutrons observed to be peaked around Li-particle motion could be attributed to the decay of the second excited state at $E^{*}=2.26$ MeV (lifetime: 2×10^{-20} s) of ^{8}Li. The fractional yields of the intermediate ^{5}He and ^{7}He ternary fission modes relative to the ''true'' ternary ^{4}He and ^{6}He modes, respectively, were determined to be 0.21(5) for both cases. The mean energy of the ^{4}He residues resulting from the ^{5}He decay was determined to be 12.4(3) MeV, compared to 15.7(2) MeV for all ternary α particles registered, and to 16.4(3) MeV for the true ternary α particles. The mean energy of the ^{6}He residues from the ^{7}He decay is 11.0(15) MeV, compared to 12.3(5) MeV for all ternary ^{6}He particles. The population of ^{8}Li* was deduced to be 0.06(2) relative to Li ternary fission, and 0.33(20) relative to the yield of particle stable ^{8}Li. The perspective of using the observed intermediate LCPs for probing the ternary scission configuration in ^{252}Cf fission with the aid of trajectory calculations is briefly discussed.

DOI: 10.1103/PhysRevC.65.044614 PACS number(s): 25.85.Ca, 24.75.+i, 23.20.En, 29.30.Ep

I. INTRODUCTION

Light-charged-particle- (LCP) accompanied fission, also known as ternary fission (TF), is a rare process ($\simeq1/260$ relative to binary fission, for ^{252}Cf) [1,2]. In TF, nucleons from the neck formed between the main fragments right at scission cluster into a light third nucleus that is ejected at about right angle to the fission axis, due to the focusing by the Coulomb field from the nascent fragments. In about 87% of ternary fission events a so-called long-range α particle (LRA) is present, characterized by a continuous (near-Gaussian) energy spectrum with $\simeq16$ MeV mean energy and $\simeq11$ MeV width [full width at half maximum (FWHM)] [3]. Other LCPs with still sizable partial yields are ^{3}H ($\simeq7\%$), the neutron-rich He isotopes ^{6}He ($\simeq3.5\%$) and ^{8}He ($\simeq0.2\%$), and the ^{7,8,9}Li ($\simeq0.5\%$) and ^{9,10,11}Be ($\simeq2\%$) nuclei. For the time being, a large variety of other much rarer species, predominantly the neutron-rich isotopes from elements up to silicon, have been measured in various thermal-neutron induced fission reactions [from ^{233}U($n_{\rm th},f$) to ^{249}Cf($n_{\rm th},f$)] [3,4]. For spontaneous fission of ^{252}Cf [^{252}Cf(sf)] no fractional isotopic yields of LCPs with $Z>3$ are hitherto available from experiment.

It is expected that LCPs are born not only in their respective ground states, but also with some probability in excited states [5,6]. In particular, in the γ-ray spectra taken simultaneously with Be LCPs and the two fission fragments in the present experiment on the TF of ^{252}Cf [7,8], the 3.37 MeV γ-ray line from the 0.18 ps disintegration of the first excited level in ^{10}Be was observed. Currently, much attention has been attracted upon the unexpected result that a fraction of the ^{10}Be γ radiation seems to appear as a non-Doppler broadened line in the γ ray spectrum, indicating that the γ decay occurs at least partially from a source at rest. More recent high-resolution data with germanium detectors seem to confirm this observation [9,10], supporting the suggestion already pointed out in Ref. [7] of the possible existence of a molecular type of nuclear structure at the scission point in ^{10}Be accompanied ternary fission [9–11]. However, for this conjecture to be true, the ^{10}Be nucleus is to be held in the potential well between the main fission fragments for an incredibly long time at least comparable to the lifetime of the ^{10}Be excited state, i.e., for $\simeq10^{-13}$ s before the system breaks up into the three charged products. Besides the interesting perspective of signaling a new type of intermediate nuclear structure, the population of excited states in the ternary particles is of considerable interest on its own, since information on the exit channel of fission, e.g., on the energy dissipation in the saddle-to-scission stage, might be inferred by measuring ratios of excited and ground states in the same LCP [8]. Experimentally, the population of excited states in LCPs can be traced also by a neutron measurement, in the

*Present address: Gesellschaft für Schwerionenforschung, D-64291 Darmstadt, Germany.
†Present address: Section Physik, Ludwig-Maximilians-Universität München, D-85748 Garching, Germany.

few cases at least when excited levels in the neutron-rich light nuclei disintegrate by neutron emission rather than by γ decay, e.g., the neutron-rich helium isotopes ^{6}He and ^{8}He, and the odd-odd lithium isotope ^{8}Li. In the present work, ^{8}Li at $E^{*}=2.26$ MeV is identified as the first case of an LCP being emitted in a neutron-unstable excited state.

Formation of LCP species in ^{235}U(n_{th},f) and ^{252}Cf(sf) that are unstable against neutron decay from their ground states was discovered already some 30 years ago in coincidence experiments between ternary α particles and neutrons. An enhancement $(27\pm2\%)$ of the neutron intensity in the direction of motion of the ternary α particles, as compared to the opposite direction, was observed first by Nefedov *et al.* [12] in ^{235}U(n_{th},f). Later Cheifetz *et al.* [13] and Graevskii *et al.* [14] measured for ^{252}Cf(sf) the neutron velocities and correlated α-particle energies at the relative emission angles around 0° and 180°. The data provided a stringent proof for the occurrence of intermediate ^{5}He which decays by neutron emission into ^{4}He close to the fissioning nucleus. The authors of Ref. [13] deduced the fractional ^{5}He yield to be 0.11(2) relative to all LRAs, and a mean energy of 12.4(9) MeV for the ^{4}He residues from the ^{5}He decay. Besides the direct measurements [13,14], the ^{5}He emission was also attempted to be inferred from the shape of the LRA energy spectrum, assuming its weak non-Gaussian low-energy tail [15,16] to be entirely due to the ^{5}He decay (see also reviews [1,2]). The conclusions from these studies were not unequivocal, and the energy distribution attributed to the ^{4}He residues in the recent work of Ref. [17] is inconsistent with the data from the neutron-α coincidence experiment of Ref. [13].

In the present work a new experimental study on ^{5}He emission in ^{252}Cf fission is presented, measuring the angular correlation of neutrons and LCPs in a wide range of mutual emission angles and with a previously unachieved statistical accuracy. Also, the angles with respect to the fission fragments were determined, and the energy spectra of all charged reaction products were deduced. As the LCPs are focused in the fragment Coulomb field about orthogonally to the fission axis, the set of kinematic parameters obtained has helped considerably to disentangle the neutrons of the LCP decay processes from the more frequent prompt fission neutrons. The latter ones are evaporated from the moving fragments and, thus, have angular distributions peaked around the fission axis. Besides the decay of ^{5}He we were also able to investigate, for the first time, the similar case of ^{7}He by identifying the neutron component that is correlated with the direction of motion of the much rarer ^{6}He particles discriminated from the α particles by a ΔE-E measurement.

The very short radioactive decay times of the neutron-unstable nuclei under study are comparable with the period of LCP acceleration ($\simeq 10^{-20}$ s) in the time-dependent Coulomb field of the fission fragments flying apart. The neutrons from intermediate LCP decay are thus a probe of the conditions at a very short time after scission. Since the neutrons are not affected by the fragments' Coulomb field, their angular distribution is the most stringent experimental quantity for probing the LCP starting conditions. After the LCP is released simple kinematics links the neutron angular and energy distributions to the velocity distributions of the LCPs during their decay, when the LCPs still experience a strong Coulomb repulsion. In the present work, these correlations have been modeled by a trajectory calculation for the measured intermediate LCPs decaying in the vicinity of the fissioning nucleus into neutrons and LCP residues.

It should be stressed that when the decay times and Q values for the neutron-unstable species can be inferred from resonance spectroscopy (as it is the case for ^{5}He, ^{7}He, and ^{8}Li* [18]) the novel kinematic data from the present work may provide valuable information about the scission configuration in ternary fission. The issue is briefly addressed in the paper.

II. EXPERIMENT

A. Experimental setup and procedure

In the present experiment [7,19], the Darmstadt-Heidelberg Crystal Ball (CB) [20], serving as a homogeneous and highly granulated 4π neutron detector, was combined with an efficient detection system for fission fragments and ternary particles. The CB is a dense spherical package of 162 large (20 cm long) NaI(Tl) crystals of high γ-ray detection efficiency ($\geqslant 90\%$) [20]. Results on γ emission in ^{252}Cf ternary fission have been reported in Refs. [7,21,22]. Simultaneously to γ rays, the CB registers neutrons from fission with a rather high efficiency of $\simeq 60\%$, mainly by the $(n,n'\gamma)$ reaction in iodine [23]. The γ rays were separated from the neutrons by a time-of-flight measurement. The neutron response of the CB, being of prime interest for the present work, is discussed in Sec. II B. Inside the CB a spherical space of 50 cm diameter is available which can accept the detectors for the fission fragments and LCPs. In the present study, the assembly of particle detectors was mounted inside a CH_4-filled spherical aluminum vessel, which also contained the ^{252}Cf sample (4×10^{3} fissions/s, thin backing) located at the center. The kinematic spectrometer CODIS (see Fig. 1, described also in Refs. [19,21]) consists of a novel Frisch-gridded 4π twin ionization chamber (IC) for measuring fission-fragment energies *and* emission angles, and of a ring of 12 ΔE-E telescopes (made from ΔE IC's and silicon p-i-n diodes, with a solid angle of $\pi/4$) surrounding one half of the fragment IC for measuring the LCPs [8]. Angular resolutions (FWHM) were $\leqslant 5°$ for both the fragments and LCPs. The respective kinetic energies and angular distributions of the particles may be correlated to the information on the neutrons (and γ rays) from the outer sphere. The number of measured coincidences between the ternary particles, fission fragments, and neutrons (and γ rays) which were registered and stored as list-mode data on tape in four weeks of measurement are listed in Table I, together with other experimental parameters for the different LCPs measured (Sec. III A). Simultaneously to TF events, 7×10^{7} binary fissions were recorded, the data acquisition rate for this event type being reduced by a factor of 1/64.

B. Neutron detection with the CB

The discrimination of neutrons from γ rays was achieved by measuring the neutron flight time from the ^{252}Cf sample

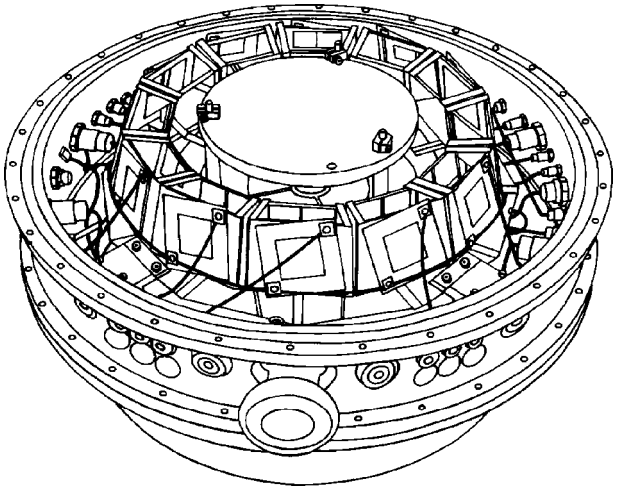

FIG. 1. Schematic view of the CODIS spectrometer with the upper part of the aluminium vessel removed. One half of the double ionization chamber is surrounded by the ring of 12 ΔE-E telescopes. The vessel was filled with CH_4 counting gas at 570 Torr. The whole setup was placed inside the hollow sphere at the center of the CB spectrometer.

to the crystals (distance 25 cm), exploiting fast timing signals from the fragment-IC cathode and from each individual CB module. For the various results on γ-ray emission, published elsewhere [21,22], narrow time windows of ± 2 ns were set onto the prompt γ-ray coincidence peaks (FWHM $\simeq 3.5$ ns) in the time-of-flight (TOF) spectra. For the neutron registration, the discrimination threshold was set at the pronounced minima in the TOF spectra between the γ peak and neutron bump, evaluating the threshold positions as a function of pulse height [24]. Since no pulse-shape discrimination is possible with NaI(Tl), the present neutron results include a small contamination ($\leqslant 10\%$) of delayed fission γ rays [25]. The calibration of the CB pulse-height spectra in terms of γ energy was performed with various γ-ray sources, following standard procedures. Since the pulse-height spectrum induced by the neutrons has no direct relation to the neutron energy, the latter has to be inferred, albeit with rather low precision, from the measured flight time (see below). As for the counting efficiency, a common threshold corresponding to 100 keV γ energy was set in all the pulse-height spectra. With similar experimental conditions, the neutron efficiency of the CB crystals was measured in an early CB design study [23] to be $\simeq 60\%$ for $E_n \geqslant 2$ MeV, dropping down to $\simeq 50\%$ for E_n below 0.5 MeV. In the present analysis, the neutron efficiency was assumed to be independent from energy. The value of $\simeq 60\%$ overall efficiency was verified in the present experiment by a comparison of the measured neutron multiplicity for ^{252}Cf binary fission with literature data. Relative efficiencies of the individual crystals, although subtending equal solid angles ($\simeq \pi/40$, each), varied by up to $\simeq 10\%$, mainly caused by the absorption in the charged-particle detectors mounted inside the CB. The corresponding corrections were derived directly from the ^{252}Cf spectra measured.

To determine the angular resolution for neutron detection (resulting from the granularity of the CB, and the cross-talk due to internal scattering) no Monte Carlo simulation (e.g., with the GEANT code) was made due to the lack of relevant cross sections data needed as an input. The problem was solved by applying a first-order correction for double hits in neighboring crystals (deduced from the measured data), and then extracting the angular response function empirically [26] by relating the measured binary-fission angular patterns of neutron-fragment coincidences to reference data [27]. The resulting angular response function $R_n(\delta)$ for the registration of neutrons by the full CB is depicted in Fig. 2, with δ denoting the angle between measured and true directions of neutron emission.

III. DATA ANALYSIS

A. LCPs and fission fragments

The good ΔE-E resolution of the particle telescopes allowed the isotope separation of H and He ternary particles, and the atomic number separation of heavier species up to carbon. The LCP energy spectra obtained with the CODIS spectrometer on the ternary fission modes with ^{3}H, ^{4}He, ^{6}He, and Li emission are displayed in the left-hand panels of Fig. 3, all spectra being corrected for energy loss in the absorber foil and the fission chamber gas. The full set of data on LCP kinetics and correlations with the measured fission

TABLE I. Spectral parameters and yields for LCPs with $Z \leqslant 3$ measured in coincidence with fission fragments. All energies in MeV. The fission neutron multiplicities $\bar{\nu}$ were also deduced from the present experiment (see Refs. [19,26]). For ^{3}H yields see text.

LCP	Events	E_{thres}	$\langle E_{\text{LCP}} \rangle$	FWHM	Yield [a]	$\langle \theta_{\text{LCP}} \rangle$/FWHM	$\bar{\nu}$
^{3}H	5.6×10^4	3	8.2(6) [b]	7.2(6) [b]	950(90)	84.5°/33.6°	2.9
^{4}He	1.3×10^6	8	15.7(2)	10.9(2)	10^4	84.1°/21.7°	3.1
^{6}He	2.6×10^4	10	12.3(5)	9.0(5)	270(30)	83.8°/19.4°	2.8
Li	2.5×10^3	17	14.3(10) [c]	14.3(10) [c]	60(10) [d]	84.9°/19.0°	2.5
(binary)	0.7×10^8	–	–	–	–	–	3.8

[a]Normalized to 10^4 LRAs.

[b]Evaluation of Wagemans [1] for ^{252}Cf.

[c]Taken from systematics, Ref. [7].

[d]Obtained from a Gaussian fit to the measured energy spectrum with fixed $\langle E_{\text{LCP}} \rangle$ and FWHM.

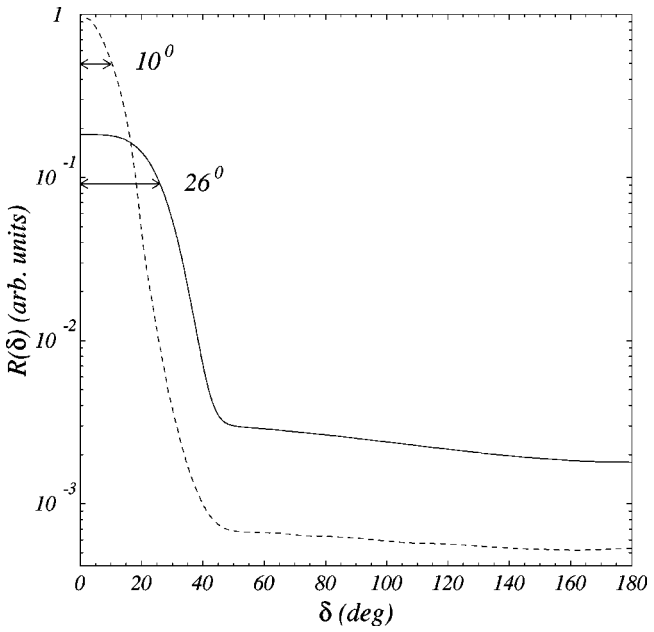

FIG. 2. Angular response functions $R_n(\delta)$ for the registration of fission neutrons (full line) with the Crystal Ball spectrometer, δ being the angle between real and measured direction of neutron emission. For comparison, the response function $R_\gamma(\delta)$ for the registration of γ rays, deduced by a GEANT simulation, is shown by the dashed line. Arrows indicate the widths of the distributions at half maximum.

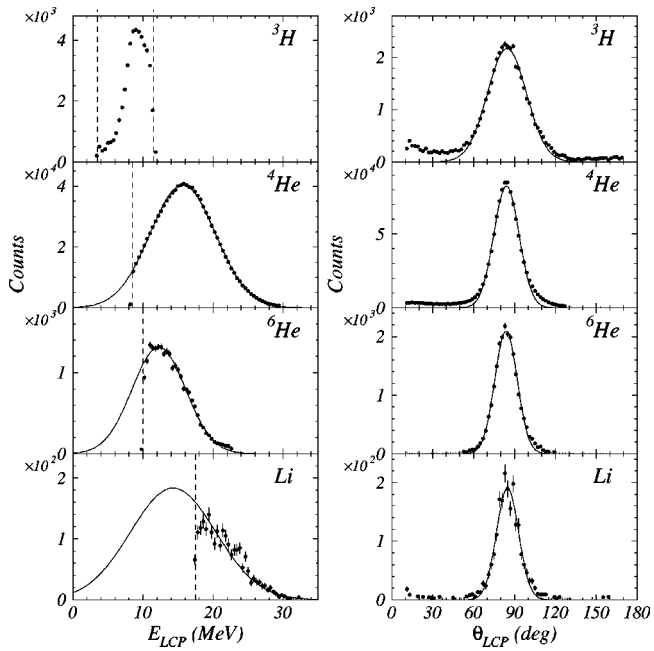

FIG. 3. *Left-hand side:* Energy spectra of ^{3}H, ^{4}He, ^{6}He, and Li LCPs. The dashed lines mark experimental low and high-energy cutoffs. *Right-hand side:* Respective angular distributions $dN/d\theta_{\mathrm{LCP}}$, with θ_{LCP} denoting the angle with respect to the direction of motion of the fission fragment from the light mass group. Solid lines are Gaussian fits. Parameters of energy spectra and angular distributions, as well as the fractional yields deduced with respect to α particles are listed in Table I.

fragments will be the subject of a subsequent article [28]. There is a lower energy limit in the LCP energy distributions because of the energy loss of the LCPs in the fragment chamber gas and an additional absorber foil protecting the ΔE-E telescopes from the intense 6.1 MeV α radiation of ^{252}Cf. The lower cutoff energy for ternary α particles is at 8 MeV, allowing us to deduce correlations with all other parameters over a wide energy range. For the heavier LCP species, the accessible range of LCP energy is more seriously limited by the cutoff. For particles heavier than ^{6}He, energies accessible to measurement exceed the most probable energies. For the ^{3}H spectrum there is also an upper limit of 11.5 MeV for full energy registration due to the limited thickness of the silicon detectors. This further imposes a strong distortion on the energy spectrum, as the high energy particles deposit only part of their energy in the detectors and are, hence, registered at lower energies. As a result, the spectral maximum is shifted and the width observed is too narrow. The data are, however, valuable for extracting ^{3}H yields.

The distributions of emission angles of the LCPs with respect to the fragment motion are displayed in the right-hand panels of Fig. 3 taking, following convention, the angle θ_{LCP} with respect to the fragment from the light-mass group. The data in Fig. 3 confirm that the LCPs are emitted preferentially at right angles to the fragment direction, as expected. The angular width $\Delta\theta_{\mathrm{LCP}}$ is getting smaller with increasing atomic number of the LCP. This tendency is known from previous data for triton and α-particle emission only [29]. It should be noted that in case the LCPs would have been measured over full energy ranges even narrower angular widths had to be expected since, as it is known from ternary α emission [30], the angular dispersion increases with the energy of the LCPs. Spectral parameters and yields for the LCPs at hand are summarized in Table I.

B. Neutron angular distributions

For the presentation of neutron angular distributions we made use of the sharp angular correlation between LCPs and fragments by sorting the measured emission angles of the registered neutrons into an *in situ* coordinate system xyz (see Fig. 4) that permits us to deduce neutron angular correlations both with respect to the direction of the fragment motion and to the emission direction of the LCPs. For the notation, the z axis was chosen to coincide with the light fragment (LF) direction. The x axis was chosen to be in the plane defined by the three charged reaction products (the fragment pair and the LCP) such that it is closest to the direction of the LCP motion. The y axis is perpendicular to the xz plane making a right-handed coordinate system xyz.

The left-hand panels in Fig. 5 give an overview of the resulting projections w_{zx} of the differential neutron yields on the plane zx in which the momenta of the LCP and the fragments are coplanar, as a function of the angle ϕ_{zx} defined in Fig. 4. The angular patterns, in coincidence with ^{3}H, ^{4}He, ^{6}He, and Li emission, show the well known emission patterns of prompt fission neutrons with maxima in the directions of the two fragments ($\phi_{zx}=0°$ and $\phi_{zx}=180°$) and

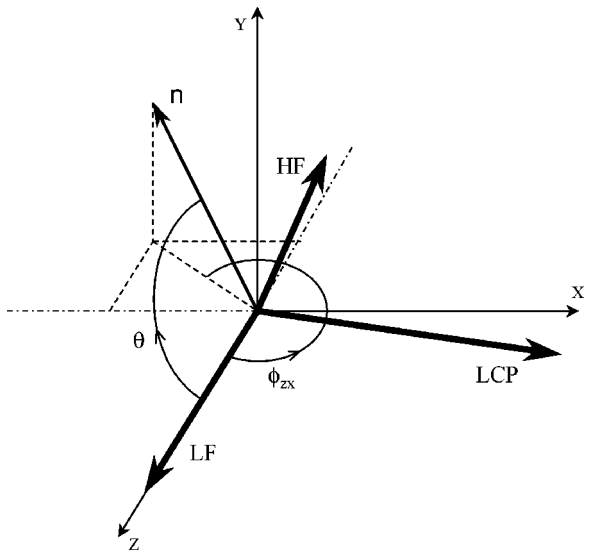

FIG. 4. Coordinate system xyz for analyzing the angular distributions of neutrons with respect to the emission direction of the LCPs and the fission fragments (LF = light fragment, HF = heavy fragment).

with the neutrons more sharply focused along the fragments from the light mass group ($\phi_{zx}=0°$). These data were used to determine the average multiplicities of fission neutrons, $\bar{\nu}$ [3,28], included in Table I. In the angular patterns obtained in coincidence with ^{4}He, ^{6}He, and Li emission the neutron intensity is higher around the LCP emission angle ($\phi_{zx} \simeq +83°$) as compared to the opposite direction. We attribute the difference in the neutron yield at the minima of the neutron angular distributions to the neutron decay of the LCPs. Note that no difference in the neutron yield between forward and backward angles with respect to the direction of motion of the LCP is observed in coincidence with ^{3}H.

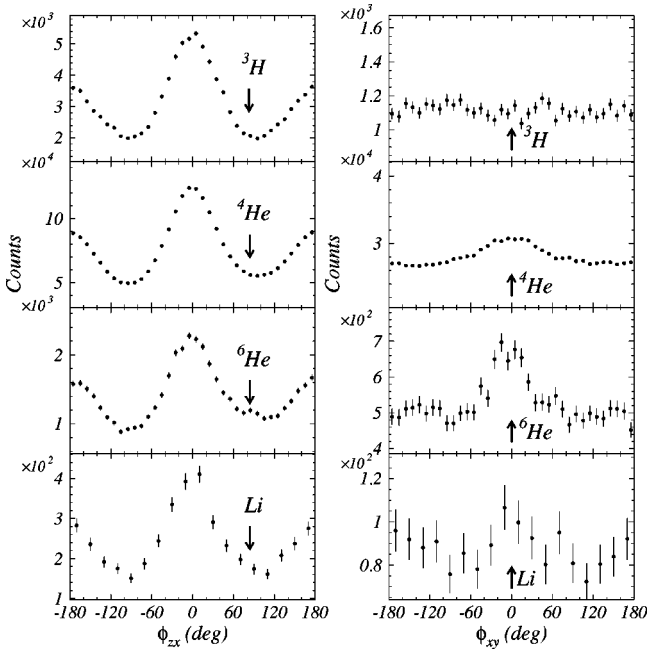

FIG. 5. *Left-hand side:* Projections w_{zx} of the measured neutron intensity on the zx plane in the coordinate system xyz (see Fig. 4) built up by the linear momenta of the fragments and LCPs. *Right-hand side:* Projections w_{xy} of the measured neutron angular distribution on the xy plane perpendicular to the fission axis, with the additional restriction that the angle θ between neutron and the light fission fragment lies in the range $90°\pm30°$. Data refer to the ^{3}H, ^{4}He, ^{6}He, and Li accompanied fission (from top to bottom). The respective directions of the LCPs are indicated by arrows.

The surplus neutrons along the direction of ^{4}He, ^{6}He, and Li motion are manifested more clearly in the projections w_{xy} onto the plane orthogonal to the fission axis and, even more, when only events are selected for which the relative angle θ between the neutron and the LF (see Fig. 4) is restricted to $60°\leqslant\theta\leqslant120°$. In this angular window prompt fission neutrons emanating from the fragments naturally have low intensity. Such conditioned projections w_{xy} of the differential neutron yield are displayed in the right-hand panels of Fig. 5 as a function of ϕ_{xy}. One observes a rather wide peak in the neutron angular distribution around the direction of ^{4}He particles, which is superimposed on the distribution of prompt fission neutrons. The angular width measured for the LCP neutrons is remarkably narrower in the case of ^{6}He and Li accompanied fission. It is noteworthy that again no sign for such surplus neutrons along the LCP direction is observed when the fission event is accompanied by a triton.

To analyze the neutron angular correlations in terms of the neutron decay from ^{5}He, ^{7}He, and Li nuclei we have calculated the angular distributions for the neutrons from the respective decays. For this purpose, the time evolution of the LCP velocity was simulated by trajectory calculations, assuming initial ternary fission configurations as given in Ref. [31] (for details see Sec. V A). As the intermediate neutron sources, the lowest neutron-unstable LCP states were assumed to be the dominant ones, i.e., the ground states of ^{5}He and ^{7}He, and the second excited state ($E^*=2.26$ MeV) of ^{8}Li (spectroscopic data are listed in Table II). Moreover, isotropic neutron emission in the LCP center-of-mass (c.m.) system was assumed, and the neutron c.m. energies were taken from the Q values.

Figure 6 illustrates the different steps in our analysis of the angular distributions of the LCP neutrons observed. The left-hand panels display the projections w_{xy} of the calculated neutron angular distributions with respect to the LCP direction, and the corresponding distributions when convoluted with the angular response function of the CB (as given in Fig. 2). The convoluted distributions were used as the fit functions to the w_{xy} data, together with a function that describes the contribution from the more frequent neutrons evaporated by the fragments (see below). The intensity ratios between LCP neutrons and prompt fission neutrons were taken as the free parameters in the fitting procedure for deducing relative yields (Sec. IV A 1). The resulting fits to the measured neutron angular distributions, with no constraints on θ angles in the cases of ^{5}He and ^{7}He (in view of the larger angular widths involved), are shown in the central panels of Fig. 6. The data are well described ($\chi^2/N\simeq1$) by the fitted curves, confirming that the above neutron-unstable nuclides are in fact produced as ternary particles. Finally the

TABLE II. Spectroscopic parameters of the neutron-unstable nuclei ^{5}He, ^{7}He, and ^{8}Li ($E^{*}=2.26$ MeV), taken from Ref. [18], observed as intermediate ternary particles in ^{252}Cf fission.

Nucleus	Resonance width Γ	Lifetime τ	Q value
^{5}He$(3/2^{-})\rightarrow$ ^{4}He$+n$	600(20) keV	1.1×10^{-21} s	0.89 MeV
^{7}He$(3/2^{-})\rightarrow$ ^{6}He$+n$	160(30) keV	4.1×10^{-21} s	0.44 MeV
^{8}Li$^{*}(3^{+})\rightarrow^{7}Li+n$	33(6) keV	2×10^{-20} s	0.25 MeV

resulting w_{xy} projections of the particular LCP neutron components are plotted in the right panels in Fig. 6, i.e., with the prompt fission neutron components subtracted.

Particular attention has been paid in the present analysis to the angular characteristics w_{xy} of the prompt fission neutrons in TF, shown as dashed lines in the central panels in Fig. 6. Since the latter neutrons dominate the total neutron intensity at all angles, their angular distribution (in the w_{xy} projections) has to be reliably established for unambiguously extracting the angular distributions and yields of the extra neutrons in question. The analysis of the prompt fission component was performed in the following way.

Due to conservation of linear momentum in the three-body TF process, the emission of LCPs imposes a noticeable recoil upon the motion of the paired fission fragments, causing their linear momenta to deviate from collinearity. This also breaks the symmetry of neutron emission with respect to the fission axis valid for the binary fission process. For ^{4}He TF, the fragment directions deviate from 180° on average by 4.5°, measured, e.g., in Ref. [30]. For ^{6}He and Li emission the angular deviations are calculated to be 5.1° and 7.1°, respectively. Taking the recoil effect into account, we have simulated the projections w_{xy} on the xy plane for the prompt fission neutrons in TF [22], using precisely known ^{252}Cf binary fission data [27] on neutron angular distributions with respect to the direction of the light and heavy fragment as the basis. As seen in the central panels of Fig. 6 (dashed lines), the LCP recoil momentum acting on the fragment motion causes the w_{xy} projections of the prompt fission neutron intensity to become slightly suppressed in the direction of the LCPs, and slightly enhanced in the opposite hemisphere. In the present experiment this behavior, though being obscured

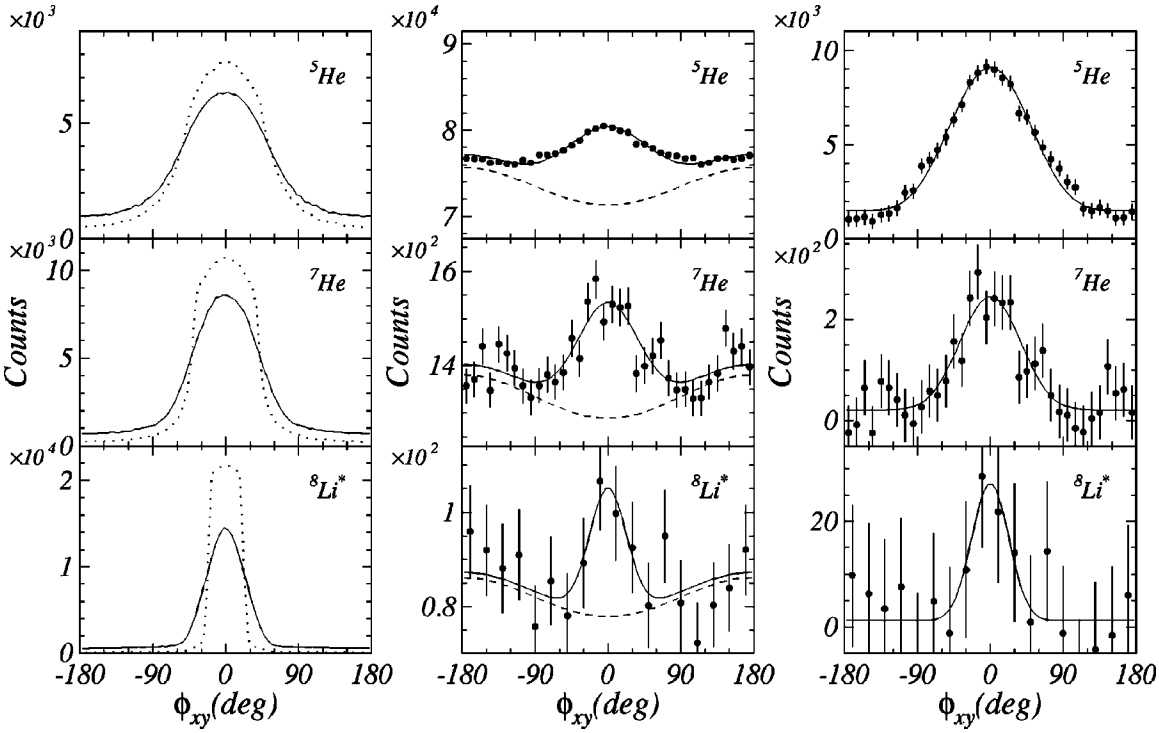

FIG. 6. Different steps in analyzing measured angular correlations of neutrons with respect to the direction of motion of ^{4}He, ^{6}He, and Li LCPs (from top to bottom): *Left-hand panel:* Neutron angular distributions w_{xy} deduced from trajectory calculations for the decay of intermediate LCPs ^{5}He, ^{7}He, and ^{8}Li*, respectively. Distributions are shown without (dotted lines) and with taking account of the experimental angular resolution (full lines). *Central panel:* Measured w_{xy} distributions, with an additional cut ($60°\leqslant\theta\leqslant120°$) being applied for the ^{8}Li* data. The solid lines represent the fits to the measured distributions with the sum of the resolution-broadened curve for LCP neutrons and the background from prompt fission neutrons (dashed lines). *Right-hand panel:* Experimental neutron angular distributions from the decay of the intermediate LCPs, compared to the simulated ones (solid lines), after subtraction of the neutrons from fission fragments. For details, see text.

TABLE III. Spectral parameters of residue particles, fractional yields, and spectral parameters for associated neutrons of the intermediate ^{5}He, ^{7}He, and ^{8}Li* ternary fission modes in ^{252}Cf(sf). All energies in MeV. The ^{5}He (^{7}He) yields are given relative to both, the true ^{4}He (^{6}He) yields and the total ^{4}He (^{6}He) yields (including residues). The ^{8}Li* yield is relative to the yield of particle stable ^{8}Li.

TF mode	$\langle E_{\rm Res}\rangle$	FWHM	Yield		$\langle\theta_{\rm LCP}\rangle$/FWHM	$E_n^{\rm max}$	$\overline{E_n}$
^{5}He	12.4(3)	8.9(5)	0.21(5) [a]	0.17(4) [b]	83.6°/22.6°	4.9 [c]	1.2 [c]
^{5}He [13] [d]	12.3(9)	–	0.12(2) [a]	0.11(2) [b]	–	–	4.0(3) [e]
^{5}He [14]	–	–	–	–	–	–	4.6(2) [e]
^{7}He	11.0(15)	8(2)	0.21(5) [a]	0.17(4) [b]	84.0°/18.2°	2.3 [c]	1.0 [c]
^{8}Li*	–	–	0.33(20)		–	2.5 [c]	1.6 [c]

[a]Relative to true ternary ^{4}He and ^{6}He particles, respectively.
[b]Relative to all ternary ^{4}He and ^{6}He particles, respectively (including residues).
[c]Derived from the trajectory calculations.
[d]For residues measured above 9 MeV threshold.
[e]For neutrons measured in the forward direction.
[f]^{8}Li($E^*=2.26$ MeV)/^{8}Li.

in the ^{5}He data because of the rather wide angular spread of the LCP neutrons, manifests itself clearly in the data for ^{7}He and ^{8}Li*. Furthermore, our treatment has also proven to be valid when analyzing the data taken for ^{3}H TF (and also for Be TF), in which case a neutron decay from LCPs evidently does not occur. It is worthwhile to note that the registration of the different LCP species in the present work was important for allowing us to check our procedure of disentangling the neutron yields from the two different sources.

IV. EXPERIMENTAL RESULTS

A. The odd-*N* helium isotopes ^{5}He and ^{7}He

1. Emission probabilities

The probability for emission of the short-lived ^{5}He and ^{7}He isotopes in ternary fission of ^{252}Cf was deduced from the ratios of LCP neutrons and prompt fission neutrons, taking for the average multiplicity of fission neutrons $\overline{\nu}$ the values of 3.1 and 2.8, deduced for the ^{4}He and ^{6}He accompanied fission modes, respectively. For ^{4}He and ^{6}He energies above the registration thresholds (8 MeV for ^{4}He, and 10 MeV for ^{6}He) we have obtained for the ^{5}He and ^{7}He yields, relative to the yields of true ternary ^{4}He and ^{6}He particles, a value of 0.19(5) each. A correction for the subthreshold events (see below) gives our final results (included in Table III) for the ratios of primary yields

$$^5\mathrm{He}/^4\mathrm{He}=0.21(5) \quad \text{and} \quad ^7\mathrm{He}/^6\mathrm{He}=0.21(5).$$

These values mean that $(17.4\pm4.0)\%$ [calculated from $21(5)/(1+0.21)\%$] of all ternary ^{4}He and ^{6}He particles observed in ^{252}Cf fission are actually residues from the ^{5}He and ^{7}He breakup reactions, respectively. We note that the emission of ^{5}He has the second highest yield among all LCPs, being only superseded (by a factor of $\simeq 5$) by ^{4}He emission, but downgrading ^{3}H (by a factor of $\simeq 2$) to the third most abundant LCP. In the present experiment $(2.3\pm0.5)\times10^5$ measured events are attributed to ^{5}He. The quoted errors represent the systematic uncertainty which was estimated conservatively from the assumptions made for the evaluation. Statistical errors are comparably low, i.e., $\simeq 0.5\%$ for ^{5}He, and $\simeq 4\%$ for ^{7}He. The stated systematic errors include the uncertainty in the procedure for the background correction (Sec. III B), and a possible difference in detection efficiency for the LCP and fission neutrons. Some uncertainties also result from the assumption that the neutron decays of intermediate ^{5}He and ^{7}He LCPs from their ground states are the only source for the neutron component observed along the direction of ^{4}He and ^{6}He particles; the present results might be affected, albeit little, by a possible formation of ^{6}He and ^{8}He LCPs in excited states that are particle-unstable with respect to the two-neutron breakup into ^{4}He and ^{6}He, respectively (see Sec. IV A 2). On the other hand, noticeable formation of intermediate ^{5}He and ^{7}He in their respective excited states (at $E^*\simeq 4$ MeV) can be disregarded since these decay modes should lead to neutron angular widths much larger than the measured ones. The present figure of 0.16(4) [$\equiv 0.19(5)/(1+0.19)$] for the ratio of ^{4}He residues from ^{5}He relative to all ternary α particles, both with energies above the experimental threshold of 8 MeV, has to be compared with the figure of 0.11(2) from Ref. [13]. In view of the quite different ways of deriving both figures the agreement is fairly good.

2. Energies of the ^{4}He and ^{6}He residues and decomposition of the ternary ^{4}He and ^{6}He spectra

For both the ^{5}He and ^{7}He accompanied fission, the good statistical accuracy of the present data has allowed us to determine energy spectra of the residual ^{4}He and ^{6}He nuclei, and, furthermore, to examine how the experimental ternary ^{4}He and ^{6}He energy spectra are composed by contributions from true LCPs and those due to the neutron-unstable precursors.

The energy distributions of the ^{4}He and ^{6}He residues were deduced from the measured energy spectra by setting constraints on the neutron angular distributions shown in Fig. 6 (central part). The projected neutron yield w_{xy} was divided into the forward region (FW) at the angles $-90°<\phi_{xy}$

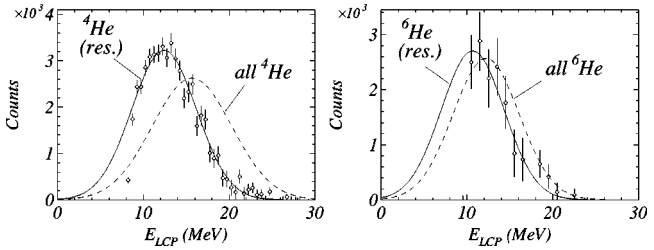

FIG. 7. Energy spectra of the ^{4}He and ^{6}He residues, gated on forward emitted neutrons. Solid lines are Gaussian fits. Dashed lines correspond to Gaussians fitted to the ungated ^{4}He and ^{6}He spectra of Fig. 2, normalized to the same areas. Spectral parameters are listed in Tables III and I. The cutoff in the LCP energy measurement is 8 MeV and 10 MeV, for ^{4}He and ^{6}He, respectively.

$<+90°$ with neutrons directed towards the LCP motion, and the backward region (BW) at the angles $\phi_{xy}<-90°$ and $\phi_{xy}>+90°$ with neutrons going in the opposite hemisphere. Coincidence ^{4}He and ^{6}He energy spectra, dN/dE_{LCP}, were then generated from the list-mode data with the conditions that neutrons were registered either in the forward or backward hemisphere. Since the energies of ^{4}He and ^{6}He residues are only weakly affected by the direction of the correlated neutrons, the energy spectra dN/dE_{Res} can in good approximation be deduced from the difference

$$(dN/dE_{\mathrm{LCP}})_{\mathrm{Res}}=(dN/dE_{\mathrm{LCP}})|_{\mathrm{FW}}-0.97(dN/dE_{\mathrm{LCP}})|_{\mathrm{BW}}, \quad (1)$$

the factor 0.97 being the corresponding FW/BW ratio for the intensity of neutrons emitted from the fragments. Figure 7 shows the resulting energy spectra for the residual ^{4}He and ^{6}He nuclei in comparison with the normal (ungated) E_{LCP} spectra for ^{4}He and ^{6}He accompanied fission, respectively.

As seen from the left panel of Fig. 7 (and the spectral parameters listed in Table III), the mean energy of the ^{4}He residues, $\langle E_{\mathrm{Res}}\rangle=12.4(3)$ MeV, is 3.3(1) MeV lower than the mean energy, $\langle E_{\alpha}\rangle=15.7(2)$ MeV, of the ungated α spectrum, and also the spectral width is somewhat narrower. The error quoted for the energy difference is smaller than those of the mean values as the latter are mainly affected by the uncertainty brought in by the energy calibration and the energy loss correction. The ^{4}He residue spectrum is well described by a Gaussian down to the 8 MeV threshold. This fact gives confidence that a substantial ^{6}He*$(2n)$ admixture to the measured ^{4}He residues can safely be excluded, since residual α's from the ^{6}He decay should have just $\simeq 8$ MeV mean energy, as estimated from the mass ratio (2/3) and the mean energy of 12.3 MeV for the ^{6}He spectrum.

The present E_{Res} spectrum is in good agreement with the previous $n-\alpha$-particle correlation experiment of Ref. [13], quoting an average energy of 12.3(9) MeV above a 9 MeV threshold. On the contrary, in the recent work by Hwang *et al.* [17], which is based on a shape analysis of single LRA spectra from different experiments [15–17], much lower mean energies (between 8.0 and 10.9 MeV) were suggested for the ^{4}He residues.

In the present work, the LRA energy spectrum of ^{252}Cf(sf) can be reliably decomposed into the components

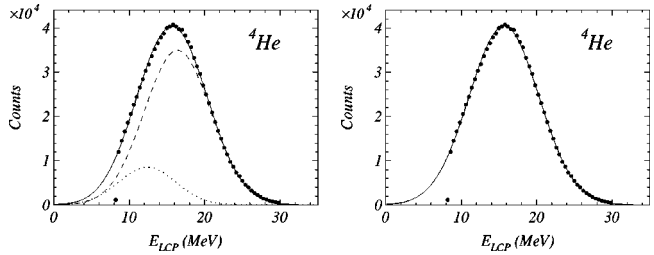

FIG. 8. *Left-hand side:* Composition of the total LRA spectrum of ^{252}Cf(sf) by true ternary α particles (dashed line) and ^{4}He residues due to the ^{5}He decay (dotted line). The energy spectrum of the ^{4}He residues from Fig. 7 and the ^{5}He/^{4}He ratio were taken as input parameters for the fit. The full line is the sum of both contributions. *Right-hand side:* Result of a single-Gaussian fit to the total LRA spectrum. Spectral parameters extracted from both fits are listed in Table IV.

from true ternary α particles and ^{4}He residues by making use of the detailed knowledge on the ^{5}He decay obtained experimentally from n-LCP coincidences. For the analysis, the results on the ^{5}He/^{4}He ratio and the first and second moments of the ^{4}He residue spectrum were taken as input parameters for performing a least-square fit with Gaussians for each of the two components, on display in the left-hand panel of Fig. 8. Fit parameters are listed in Table IV. It is important to note that the resulting mean energy for true ternary α particles, 16.4(3) MeV, is in fact 0.7(1) MeV higher than the mean energy of the composite LRA spectrum usually measured.

On the other hand, the asymmetry in the LRA spectrum caused by the ^{4}He residues is not substantial. For demonstration, a fit of the measured LRA spectrum (above 8 MeV threshold) by a single Gaussian is shown in the right panel of Fig. 8. As can be seen, the measured spectrum can be represented satisfactorily also by a single Gaussian, with a 0.6 MeV larger width than that of the true ternary α spectrum. Both single and double Gaussian fits yield about the same χ^2/N, showing that the LRA spectral shape alone is hardly adequate for disclosing the ^{5}He contribution, as attempted in Ref. [17]. The deviation from unity for the χ^2/N values obtained may be caused either by the omission of systematic errors (on the energy axis) for the fits, or rather indicate that LCP spectra may generally deviate, albeit little, from a pure Gaussian shape. Extrapolation of both fitted spectra to zero energy does not yield a substantially higher α-particle intensity of the composite spectrum at lower energies ($E_{\alpha}<10$ MeV) compared to that deduced from a single Gaussian fit. So, an enhanced yield of low-energy ternary α's, frequently discussed in the relevant literature (see, e.g., Refs. [1,2]), cannot be explained by the occurrence of ternary ^{5}He alone.

The corresponding data obtained in the present study of the ^{7}He decay (right panel in Fig. 7) yield the difference in the mean energies between the ^{6}He residues (from ^{7}He) and the ungated ^{6}He LCPs to be $\simeq 1.6$ MeV only. The spectral parameters deduced are included in Table IV. We note that the energy distributions fitted by Gaussians for both the true and residue particles have been used to correct the measured

TABLE IV. Composition of the ternary ^{4}He and ^{6}He energy spectra in ^{252}Cf(sf) by true ternary particles and the residues due to the n decay of ^{5}He and ^{7}He, respectively. Experimental data are compared with results from the trajectory calculation performed. All energies in MeV.

	Experiment			Calculation	
LCP	$\langle E\rangle$	FWHM	χ^2/N	$\langle E\rangle$	FWHM
^{4}He	15.7(2)	10.9(2)	5.9 [a]	–	–
true ^{4}He	16.4(3)	10.3(3)	6.6 [b]	14.4	18.2
Residues from ^{5}He [c]	12.4(3)	8.9(5)	–	11.1	11.0
^{6}He	12.3(5)	9.0(5)	2.2 [a]	–	–
true ^{6}He	12.6(5)	8.9(5)	2.2 [b]	9.9	10.5
Residues from ^{7}He [c]	11.0(15)	8(2)	–	8.6	8.6

[a]Fit with one Gaussian.
[b]Fit with two Gaussians, taking the measured energy spectra and fractional yields of the residues as the input.
[c]Experimental values determined from n-LCP coincidences (Sec. IV A 2).

^{5}He/^{4}He and ^{7}He/^{6}He yields for below-threshold events (see above).

We have also attempted to evaluate the difference in the LCP spectra between forward and backward emitted neutrons [according to Eq. (1)] for the data measured on ^{3}H accompanied fission. No signature for any n-^{3}H correlation was found which could have been a hint for the occurrence of intermediate ternary ^{4}H. These data, on the other hand, prove the validity of our analysis of the fission neutron part using the w_{xy} projections (Sec. III B).

3. Angular distributions of the ^{4}He and ^{6}He residues with respect to fragment motion

A similar procedure as above was applied for examining the angular distribution $dN/d\theta_{\rm LCP}$ of the ^{4}He and ^{6}He residues with respect to fragment motion. The spectra were generated in analogy to Eq. (1) by

$$(dN/d\theta_{\rm LCP})_{\rm Res}=(dN/d\theta_{\rm LCP})|_{\rm FW}-0.97(dN/d\theta_{\rm LCP})|_{\rm BW}. \tag{2}$$

The resulting distributions are shown in Fig. 9, and compared to the ungated spectra shown already in Fig. 3. Mean emission angles $\langle\theta_{\rm LCP}\rangle$ and angular widths are listed in Table III. Within experimental errors, there is no difference between the gated and ungated angular distributions. Apparently, the relatively low neutron c.m. energies do not change the emission patterns of the residues significantly which are at least in the case of ^{5}He still under strong influence of the fragment Coulomb field (see Sec. V A).

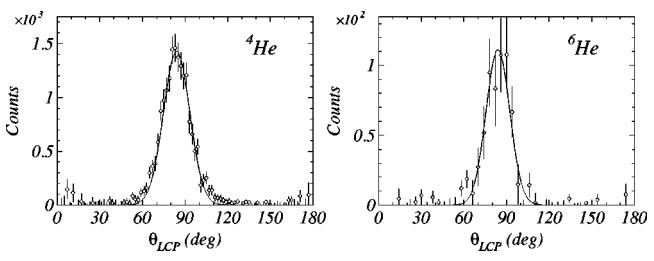

FIG. 9. Angular distributions $dN/d\theta_{\rm LCP}$ of the ^{4}He and ^{6}He residues, with $\theta_{\rm LCP}$ denoting the angle with respect to the light fission fragment. Solid lines show the corresponding ungated distributions from Gaussian fits to the data of Fig. 2, normalized to the same areas.

4. Neutron time-of-flight spectra

In an analogous manner, the time-of-flight spectra $(dN/d{\rm TOF}_n)_{\rm Res}$ of the neutrons associated with the in-flight decay of the intermediate ^{5}He and ^{7}He LCPs were generated from the difference

$$(dN/d{\rm TOF}_n)_{\rm Res}=(dN/d{\rm TOF}_n)|_{\rm FW}-0.97(dN/d{\rm TOF}_n)|_{\rm BW}. \tag{3}$$

The results for ^{4}He and ^{6}He accompanied fission modes are shown in Fig. 10, in comparison with the ungated TOF spectra representing the dominant prompt fission neutrons. In Fig. 10 the mean flight times corresponding to 1 MeV and 4 MeV neutron energies are marked by arrows. The data indicate a relative enhancement of the $(dN/d{\rm TOF}_n)_{\rm Res}$ spectra for decay neutrons at high neutron energies. The result on ^{5}He appears to be consistent with data from Refs. [13,14], stating the mean energy of the difference spectrum between narrow forward and backward angles to be 4.0(3) MeV in Ref. [13], and 4.6(2) MeV in Ref. [14], respectively. In these experiments, the neutron flight paths were 2 to 3 times longer (60 cm in [13], and 100 cm in [14]) than the effective path

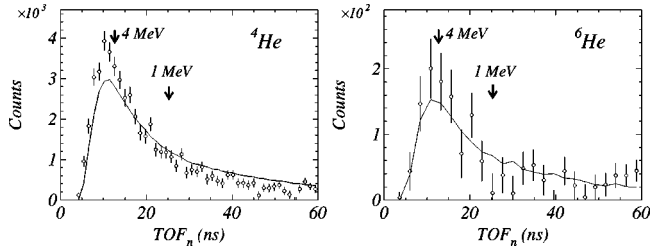

FIG. 10. Neutron time-of-flight spectra $dN/d{\rm TOF}_n$ correlated with ^{4}He (left panel) and ^{6}He (right panel) residues, for forward emission angles. Solid lines show the corresponding ungated distributions, normalized to the same areas. The neutron energies marked by arrows were calculated from the distance of 35 cm between source and mean neutron penetration depth in the NaI crystals.

lengths from 25 cm to 45 cm that the CB geometry and the 20 cm long crystals allowed for the present measurement. For the above TOF data no attempt was made to extract neutron energy spectra because of the rather limited resolution. The information on the ^{5}He and ^{7}He neutron energies will be inferred, although in an indirect way, from the trajectory calculations performed for describing the measured neutron angular distributions (see Sec. V A).

B. ^{8}Li neutron decay from the 2.26 MeV excited state

The probability of populating the short-lived 2.26 MeV ^{8}Li excited state in ^{252}Cf(sf) was deduced as described above from the measured ratio of LCP neutrons to prompt fission neutrons, for events gated on Li particles. For Li-accompanied fission, the average number of fission neutrons $\overline{\nu}$ was measured to be $\simeq 2.5$. Since a discrimination of Li isotopes was not possible with the ΔE-E method applied, we can evaluate from the present data only the yield of ^{8}Li* relative to the Li element yield, $^{8}\mathrm{Li}^{*}/\mathrm{Li}=0.06(2)$. However, relying on published isotope yields for ^{7}Li, ^{8}Li, and ^{9}Li (Ref. [32]) which result in a relative isotopic ^{8}Li yield of $^{8}\mathrm{Li}/\mathrm{Li}=0.19(10)$, the probability of populating the 2.26 MeV excited state in ^{8}Li relative to particle stable ^{8}Li (sum of the ground state and a contribution of the γ-decaying first excited state) can be estimated as

$$^{8}\mathrm{Li}(E^{*}=2.26\ \ \mathrm{MeV})/^{8}\mathrm{Li}=0.33(20).$$

Here, the rather large error is dominated by the poor statistics, and by the still bad knowledge on the ^{8}Li isotopic yield. Moreover, we have also not performed any correction for subthreshold events ($E_{\mathrm{Li}} \leqslant 17$ MeV) since counting statistics did not permit a detailed analysis of the spectral shapes.

V. DISCUSSION

A. Comparison with trajectory calculations

In the course of the past $\simeq 50$ years of intense research on ternary fission there have been numerous attempts of interpreting experimental results based upon trajectory calculations (see review [3]) that solve the classical equations of motion for the LCP and fragments in their mutual Coulomb field after the cessation of nuclear interaction. These calculations provide the link between the initial phase space conditions at scission and the kinematic parameters observed experimentally. Indeed, many investigations on α-particle TF were motivated by the perspective of providing valuable insight into the fragments scission-point configuration and getting access to prescission dynamics. The conclusions on initial dynamical parameters, however, drawn from analyzing experimental data on energy-angle correlations with trajectory computations have not yet been unequivocal because of the complexity of the problem. As pointed out in both previous ^{5}He studies [13,14], the short-lived ^{5}He TF might nevertheless be a favorable case, since LCP decay proceeds mostly at a time at which the fragments and ^{5}He nuclei are still close to each other and the decay neutrons are not affected by the Coulomb fields of fragments and LCPs. The neutron emitted from ^{5}He is thus a probe of the conditions at a time $\simeq 10^{-21}$ s after scission.

As already stated, it is in particular the angular distribution of the neutrons, as measured in the present work, that is carrying the information wanted. As shown in Sec. III B, the present data exhibit a characteristic change in the neutron angular width for the three cases studied, viz. ^{5}He, ^{7}He, and ^{8}Li*. Under the customary assumption of similar initial conditions for the three LCPs, the observed variation of the angular widths (Fig. 6) can easily be understood in terms of the LCP decay times and Q values: The ^{5}He nuclei decay nearest to the fissioning nucleus because of the short lifetime compared to both other LCPs and, related to that, have gained the least velocity. Furthermore, the neutron c.m. energy resulting from the Q value (see Table II) is comparably high. Both effects lead to a rather wide neutron angular distribution in the laboratory system, in agreement with the observation. For ^{7}He, the lifetime being a factor of about 4 longer and the Q value being down by a factor of 2, the neutron angular width becomes remarkably smaller than for the ^{5}He neutrons. Finally, the factor of 5 longer lifetime of ^{8}Li* and the low Q value of 0.25 MeV lead to an even sharper peaking of the emitted neutrons at the direction of the Li particles.

In the following we are going to describe, in more detail, the adopted ternary scission configuration that has served as the basis for calculating the LCP trajectories during acceleration and, from that, the neutron angular distributions used in the data analysis performed above (Sec. III B). However, we want to note that a comprehensive discussion on the many details of this rather complex task is not possible within the frame of the present article. In our approach, the initial conditions for the ternary scission configuration were taken basically from the work of Baum [31], who aimed at finding a semi-empirical solution which coherently matches with energy spectra of a large set of LCPs (up to $Z_{\mathrm{LCP}}=8$), measured in TF of $^{235}\mathrm{U}(n_{\mathrm{th}},f)$. The three-particle configuration at scission is accordingly modeled as indicated in Fig. 11 by spherical prefragments, scaling the radii conventionally with the fragment mass number A using $r_A=r_0A^{1/3}$.

As pointed out in Ref. [31], from classical arguments on energy conservation there are constraints for the three-particle positions near scission, imposing a distinct relation between the interfragment distance and the location of the LCP starting point. The left-side panel in Fig. 11 illustrates the assumed starting situation for α-particle-accompanied TF. The LCP is conjectured to be born in a plane oriented perpendicularly to the interfragment axis and placed midway between the tips of the two fragments. The displacement from the fission axis of the α-particle starting point, δ_0^{LCP}, is plotted in Fig. 11 versus the fragment tip distance d^{FF}. As indicated, small values of d^{FF} ($\leqslant 5$ fm) have to be excluded since they lead to high fragment kinetic energies exceeding the ternary fission Q value. For energetically allowed configurations the LCPs generally start somewhat off-axis ($\delta_0^{\mathrm{LCP}}>0$). The lines in Fig. 11 indicate the locations of possible δ_0^{LCP} and d^{FF} values that would lead to characteristic

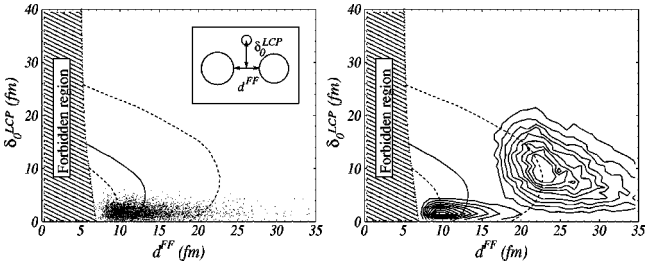

FIG. 11. *Left-hand side:* Ternary fission configuration as assumed starting situation for calculating trajectories of ternary α-particles, parametrized as α particle offset δ_0^{LCP} versus interfragment distance d^{FF}. The shaded area indicates the energy forbidden region. The solid line corresponds to possible initial configurations for which the calculated energy matches the experimental mean α-energy $\langle E\rangle$. The dashed lines to the right and left indicate configurations leading to final energies $\langle E\rangle+\frac{1}{2}$FWHM and $\langle E\rangle-\frac{1}{2}$FWHM, respectively. The distribution of starting positions of α particles and fragments adopted for the trajectory calculation in the present work are displayed as scatter plot. *Right-hand side:* The same situation assumed for intermediate ^{5}He emission. The wider contour plot at the right illustrates how particle and fragment positions have developed at time $t=1.1\times10^{-21}$ s, corresponding to the lifetime τ of ^{5}He.

energies of the α-particle spectrum when the initial momentum of the α particle, perpendicular to the fission axis, is taken to be a fixed value σ_p, which is estimated from δ_0^{LCP} by applying the Heisenberg uncertainty principle ($\sigma_p\delta_0^{\mathrm{LCP}}=\hbar$).

It is worthwhile to note that from more sophisticated modeling of the initial TF configuration with consideration of effects involving the stretching of the fissioning nucleus prior to scission by relevant shape parametrizations there are well founded theoretical arguments for locating the LCP starting positions off-axis. As an example, in the recent work of Mişicu *et al.* [33] the issue was interpreted in a quasimolecular picture, with the fission fragments developing almost collinear and the light particle orbiting in the neighborhood of the equatorial region. In α-particle cluster emission models (e.g., Refs. [34,35]) placing the LCP starting point off-axis is regarded as allowing the LCP trajectory to start at an exit point from the nascent fragments' nuclear potential, i.e., the vertex where the LCP overcomes the Coulomb barrier from the fragment pair at that moment. In a sense, the classical calculation adopted in the present work takes LCP trajectories into account from the exit points onwards.

For the purpose of simulating LCP trajectories in the present approximation some refinements in the choice of the initial conditions compared to Ref. [31] were, nevertheless, made. The calculations were performed with the following starting conditions:

(a) The distances d^{FF} between the fragment surfaces were distributed following Ref. [31] as an exponential function, with a minimum distance $d_{\mathrm{min}}^{\mathrm{FF}}$ given by the diameter of the LCP when placed just midway between the fragments ($d_{\mathrm{min}}^{\mathrm{FF}}=2\times1.2A_{\mathrm{LCP}}^{1/3}$ fm):

$$P(d^{\mathrm{FF}})=e^{-\mu(d^{\mathrm{FF}}-d_{\mathrm{min}}^{\mathrm{FF}})}. \tag{4}$$

(b) The LCP offsets were distributed as a two-dimensional Gaussian in the plane of emission leading to

$$P(\delta_0^{\mathrm{LCP}})\propto\delta_0^{\mathrm{LCP}}e^{-1/2(\delta_0^{\mathrm{LCP}}/\sigma)^2} \tag{5}$$

as the distribution for the off-axis displacement δ_0^{LCP}. The parameters μ and σ in Eqs. (4) and (5), respectively, which depend on the LCP radii in different ways, were taken as deduced empirically in Ref. [31] from a fit of a number of measured LCP spectra.

(c) A distribution for the initial LCP energies E_0^{LCP} was introduced, which corresponds to that of the LCP linear momenta related to the δ_0^{LCP} distributions by the Heisenberg principle.

(d) Fragment mass splits were allowed to vary within the margins of the measured fragment mass distribution [19].

(e) For each fragment mass split and initial ternary spatial configuration the Q value and the three-body potential Coulomb energy V were calculated and only those initial conditions were selected, for which the energy balance $Q-V-E_0^{\mathrm{LCP}}$ was positive.

(f) For the remaining configurations, the available energy at scission $Q-V-E_0^{\mathrm{LCP}}$ was attributed to the fission fragments, and was randomly partitioned into the fragment total excitation energy (TXE) and prescission kinetic energy E_0^{FF}. This selection accounts for the customary view that with increasing elongation of the fragment scission configuration (corresponding to small values of V) both, the TXE and E_0^{FF} increase on the average. Considering the fragment excitation energy TXE in the energy balance at scission (which partly compensates for the approximation of taking a spherical prefragment) was shown in Ref. [31] to be important for reproducing measured energy correlations between fragments and LCPs [30]. The resulting distribution of E_0^{FF} provides the starting fragment energies E_0^{LF} and E_0^{HF}.

(g) Trajectories for both, the fragments and LCPs (the latter being assumed to come into existence right at scission), were calculated by solving the classical equation of motion in the common Coulomb field. The distribution of starting positions for fission fragments and ^{4}He (^{5}He) LCPs at this step of the calculation is inserted as a scatter (contour) plot in Fig. 11.

(h) As for the intermediate ^{5}He, ^{7}He, and ^{8}Li* LCPs, their exponential decay (according to the mean lifetimes τ) was taken into account immediately when acceleration starts. After neutron decay, the trajectories of the further accelerated residues were followed.

Figure 12 displays the resulting time evolution of average LCP velocities for the intermediate ^{5}He, ^{7}He, and ^{8}Li* particles, which were used for simulating the angular distribution of the decay neutrons (Sec. III B). Crosses in Fig. 12 mark mean velocities at the average decay times τ. At time τ, the ^{5}He particles have gained a fraction of 65%, on average, from the maximum velocity at large distance. This corresponds to an average energy of $\simeq5$ MeV at the time of breakup. The authors of Ref. [13] deduced a value of 6.3(8) MeV from the energies of residues and neutrons measured at the forward angles investigated. At time τ, the ^{5}He nuclei

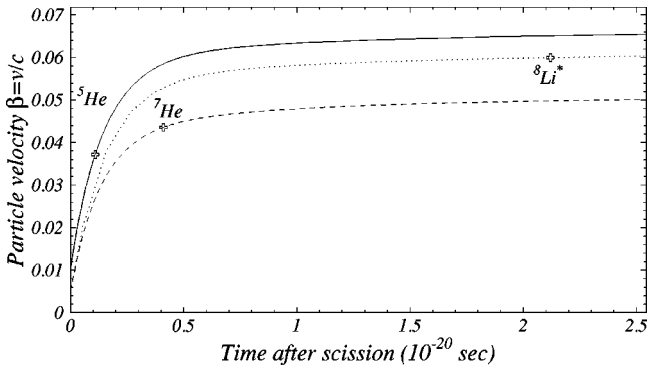

FIG. 12. Time dependence of mean velocities during acceleration for the intermediate ^{5}He, ^{7}He, and ^{8}Li* LCP particles, deduced from trajectory calculations. Crosses indicate mean velocities at the lifetime τ for each isotope.

are, on the average, only $\simeq 12$ fm from the starting positions; the right-hand panel in Fig. 11 illustrates the distribution of the ^{5}He and the fragment positions at times $t=0$ and $t=\tau$. As for the longer-lived ^{7}He and ^{8}Li* ternary particles the corresponding average distances at the mean lifetimes τ are already 40 fm and 330 fm, and the fraction of the final velocities they have gained at these distances are 90% and 99%, respectively.

A crucial test for the assumptions made in the trajectory calculations is how well the measured LCP energy distributions are reproduced. This is demonstrated in Fig. 13, where calculated energy spectra are displayed, both for true ternary α particles and ^{4}He residues, and also for true ^{6}He particles and ^{6}He residues (values are included in Table IV). Compared to the data shown in Fig. 7, the simulated spectra somewhat underestimate the mean energies and overestimate the widths. There is also some deviation from a Gaussian shape in the spectrum of ^{4}He residues which might be rather due to the limited accuracy of the calculations than being a real effect. Nevertheless, the overall agreement is fairly good. In particular, the measured energy shifts between true ternary particles and residues are correctly described by the calculation.

The satisfactory description of the data on the intermediate ^{5}He and ^{7}He TF modes concerning neutron angular distributions and energies of residues also gives confidence in the neutron energy distributions obtained after the transformation from the intermediate particles' c.m. system to the laboratory system. The results are shown in Fig. 14, where the calculated neutron spectra, multiplied by the corresponding residue yields relative to binary fission, are compared with the ^{252}Cf prompt fission neutron spectrum. Calculated maximum energies $E_n^{\max}$ and average energies $\overline{E_n}$ for the LCP neutrons are listed in Table III. It should be noted that the surprisingly sharp drop of the neutron spectrum at high energies is due to the particular kinematics of neutron decay for an emitter which is being accelerated. For ^{5}He TF the average energy $\overline{E_n}$ is 1.2 MeV, as compared to 1.9 MeV for the prompt fission spectrum. The low value for $\overline{E_n}$ only seemingly contradicts the figures exceeding 4 MeV quoted in Refs. [13,14]. Neutron energies of $\simeq 4$ MeV coincide with the high-energy part in the calculated spectrum in Fig. 14 and result from neutrons emitted at near forward angles with respect to the ^{5}He direction. Only forward angles were in fact measured in Refs. [13,14]. At this point it is important to note that all neutrons emitted into 4π in the LCP c.m. system were taken into account by our procedure used for fitting the angular distributions of neutrons and deducing the intermediate particle yields (Secs. III B and IV A 1). However, for deriving experimental parameters of residue particles, as e.g., the energy spectra given in Secs. IV A 2–4, it is sufficient to consider only that fraction of the decay processes where the neutrons are mainly emitted towards forward angles with respect to the LCP direction.

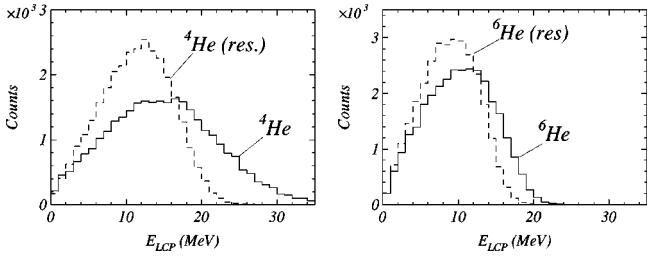

FIG. 13. *Left-hand side:* Calculated energy spectra for true ternary α particles (full line) and residual ^{4}He particles from the ^{5}He decay (dashed line). *Right-hand side:* The same spectra for true ^{6}He and residual ^{6}He particles from the ^{7}He decay. The corresponding experimental data are displayed in Fig. 7. Measured and calculated spectral parameters are compared in Table IV.

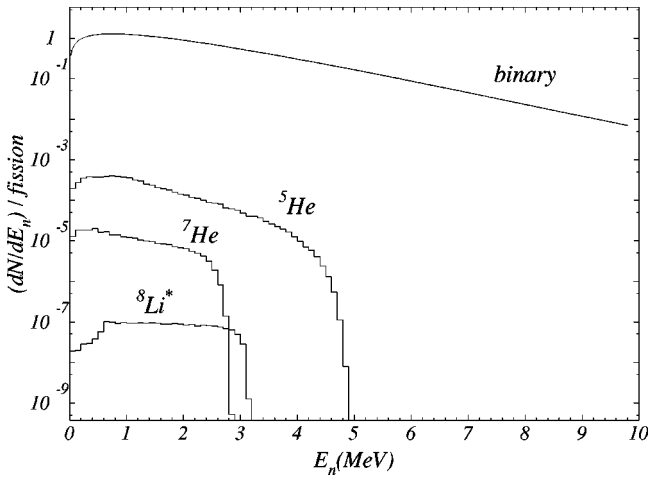

FIG. 14. Simulated neutron energy distributions from intermediate ^{5}He, ^{7}He, and ^{8}Li* decay, in comparison with the standard ^{252}Cf fission neutron spectrum (labeled "binary"). Intensities are normalized to binary fission according to the fractional yields determined in the present work. Average and maximum energies of LCP neutrons are listed in Table III.

In summary, the present study on the scission configuration provides a widely consistent picture of the energetics and dynamics furnished by the intermediate LCPs at very short times after the system's separation. It is believed that the fragment configurations used as a starting point in our calculations are representative. However, at the present stage of our investigation no attempt has been made to extract,

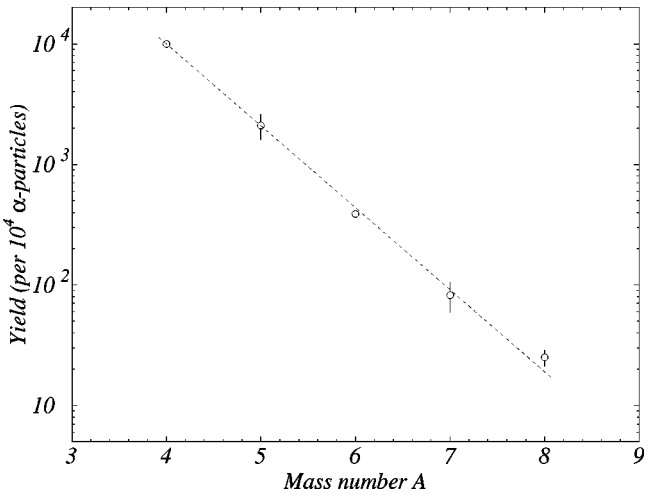

FIG. 15. Fractional yields for helium LCPs in ternary fission of ^{252}Cf(sf) for the isotopic chain $4 \leqslant A \leqslant 8$, normalized to 10^4 α particles. The ^{6}He and ^{8}He yields are taken as averages from published data [35–37]. The straight line is to guide the eye.

vice versa, from the measured data characteristic scission point parameters such as the value for the initial fragment energy E_0^{FF} (as was attempted in Ref. [13]). In the evaluation of the latter quantity the deformation of the fissioning system at scission can no longer be neglected as it was done for the purpose of the present analysis.

B. Yield systematics of the He isotopes ($4 \leqslant A \leqslant 8$) in ternary fission

The present data on the emission probabilities of the odd-N helium isotopes ^{5}He and ^{7}He in the TF of ^{252}Cf permit to establish the yield systematics for the helium isotopic chain for mass numbers from 4 to 8, by using in addition data from literature for the ratios ^{6}He/^{4}He and ^{8}He/^{4}He for even-N isotopes (Refs. [32,36,37]). The yields are displayed in Fig. 15. Surprisingly, there is no neutron even-odd effect observed in the helium particle yields. A neutron even-odd effect, superimposed on a more pronounced proton even-odd effect, is known to characterize the yields of particle-stable LCPs from other elements; the emission of even-N isotopes is generally found to be favored compared to their odd-N neighbors [3].

The rather high ^{5}He/^{4}He and ^{7}He/^{6}He ratios of 0.21 each deduced in the present work are also not borne out by available theories [38–40]. The LCP yields are usually estimated from the ''standard'' formula, which results from quite different theoretical approaches [38–40]:

$$Y_{\mathrm{LCP}} \propto \exp[(Q-V)/T]. \tag{6}$$

Here Q denotes, as in Sec. V A, the total energy release in ternary fission. For yield calculations often a single fragment mass split is chosen with a common heavy fragment around the doubly magic ^{132}Sn that maximizes Q. The potential energy V at scission is calculated for a configuration with an educated guess for the location of the LCP between the two fragments. In fitting Eq. (6) to experimental data, the denominator, denoted as an ''effective temperature'' T in Refs. [38,39], or as an ''action integral'' Γ in the adiabatic approach of Ref. [40], is used as a free parameter. By applying Eq. (6) a ^{5}He rate of only about 5% relative to ^{4}He is estimated, which is a factor of 4 smaller than observed.

This discrepancy is solved when considering, besides the energetics at scission, also the spins of the LCPs. In a systematic statistical approach, theoretical yields should be multiplied with the statistical weight factor, $(2I_i+1)$, with I_i being the spin of the LCPs in states i. This was proposed earlier by Valskii [6], who established an interpolation formula for the description of relative LCP yields. The formula works rather successfully for atomic numbers $Z \leqslant 8$. In that work also the population of excited levels (up to $\simeq 5$ MeV) was considered. In the LCP-yield calculation the resulting yields for excited states were added to the respective ground-state yields in case of γ decay, or to the ground-state yields of the neighboring isotopes $(Z,A-1)$ in case of neutron emission.

Following this view, the yield formula in Eq. (6) is generalized by taking into account excited states and spin multiplicities of the LCP:

$$Y_{\mathrm{LCP}} \propto \sum_i (2I_i+1)\exp[(Q-V-E_i^*)/T]. \tag{7}$$

With this ansatz, theoretical yield ratios ^{5}He/^{4}He, and ^{7}He/^{6}He will increase by a factor of about 4 due to the $3/2^-$ spin of the ^{5,7}He ground states as compared to the 0^+ spin of ^{4,6}He. Thus, the consideration of the multiplicity of the LCP states brings the calculated yields into close agreement with the present experimental data. The accuracy of Eq. (7) for calculating the LCP yields is, however, still questionable [41]. While the spin statistic and the population of excited LCP states should be accounted for in calculating LCP yields, the simplifications generally made in deducing the energy terms Q and V result in substantial ambiguities in the evaluation of the parameter T (or Γ [40]). It is evident that accurate data on the relative population of states in the same LCP would allow to obtain more reliable estimates for T (or Γ). Moreover, in most of the available TF theories the preformation probability of the LCP clusters is disregarded which, as concluded from recent systematic studies [42], seems to influence the LCP yields as well. In this context, it would be interesting to investigate whether ''exotic'' clusters as ^{5}He and ^{7}He (with an ''unbound'' neutron attached weakly to a nuclear core) can be treated as the stable species inside the parent nucleus or whether some final state interaction with neutrons from the surrounding nuclear matter might come into play when setting free the ternary ^{5}He and ^{7}He particles.

VI. SUMMARY AND CONCLUSIONS

We have investigated the formation of the neutron-unstable ^{5}He, ^{7}He, and ^{8}Li nuclei in ternary fission of ^{252}Cf by an angular correlation measurement of neutrons, fission fragments, and LCPs. The use of highly efficient angle-sensitive detectors for all particles has yielded valuable in-

formation on emission probabilities and kinematic parameters. The present results on ^{5}He confirm and supplement earlier work [13,14], while the intermediate ^{7}He and ^{8}Li* LCPs were identified for the first time.

The full angular distributions of neutrons with respect to LCP motion were measured for the first time in the present experiment. The data could be well reproduced by trajectory calculations for the LCP motion and by simulating their subsequent neutron decay according to known spectroscopic data. The ^{5}He and ^{7}He data could be well described by the formation of these nuclei in the neutron-unstable ground states; other conceivable LCP decay channels, such as the two-neutron breakup reactions of excited ^{6}He and ^{8}He nuclei, are assumed to give only minor contributions to the neutron yields observed. The measured energy spectrum for the ^{4}He residues from the ^{5}He decay does support this assumption.

It is worthwhile to note that ternary fission with the emission of neutron-unstable LCPs provides a source of neutrons that are emitted at about right angles to the fission axis. The dominant part of LCP neutrons comes from ^{5}He (see Fig. 14) with about one neutron in every 1500 binary fission events. This is only one order of magnitude below the currently accepted yield of 0.011(3) for so-called scission neutrons from ^{252}Cf binary fission [43], i.e., the ^{5}He neutrons mimic at least part of those early neutrons thought to be related to the binary fission process. As inferred from trajectory calculations, the kinetic energy distribution of ^{5}He neutrons has only a slightly different spectral shape as compared to the prompt fission neutrons, the energies being limited, however, to $E_n < 5$ MeV (Fig. 14).

The remarkably high intensity of ^{5}He emission in ^{252}Cf fission urges one to think about more extended and precise experimental studies of this TF mode. Modern neutron detector arrays, such as the DEMON setup [44], combined with particle detectors similar to CODIS, would permit to measure angular *and* energy distributions of neutrons from the ^{5}He decay with considerably higher precision than in the present work. These studies should aim at covering the complete kinematics of the decay, which will have to be traded off with a lower counting efficiency than that of the CB used in the present experiment and, consequently, will require the use of stronger sources.

As shown in Fig. 8, the residual ^{4}He nuclei from the ^{5}He decay contribute to the ternary α-particle spectrum mainly at low energies. However, the asymmetry in the ternary α-particle spectrum imposed by the ^{5}He decays was shown to be rather weak. Hence, the present analysis indicates that the frequently discussed enhancement of α-particle yield at low energies ($E_\alpha < 10$ MeV) compared to a Gaussian shape (see, e.g., Refs. [1,2]) cannot be fully attributed to the ^{5}He emission. On the other hand, the mean energy of true ternary α particles in ^{252}Cf fission was found to be 0.7(1) MeV higher than the energy usually determined by experiments without discrimination between true and residue α particles. It is worthwhile to note that the present result with about 17% of registered α particles being actually due to ^{5}He emission also implies that LCP yield systematics have to be corrected accordingly; for practical reasons LCP yields are often normalized to the yield of the ternary α particles [1–3].

Neutrons coming along with Li particles were found to have quite a narrow angular distribution peaked along the Li-particle motion. Well supported by trajectory calculations, these neutrons are attributed to the decay of the second excited state ($E^* = 2.26$ MeV) in ternary ^{8}Li. This is clear evidence for the formation of excited particle-unstable LCP states. A more detailed theoretical analysis should also consider the population of the γ-decaying 0.98 MeV first excited state in ^{8}Li and higher-energy neutron-unstable states with $E^* \geqslant 3.21$ MeV. Also, neutron decay branches from ^{10}Li and ^{11}Li cannot be excluded to have contributed to the measured LCP neutrons, although those contributions are expected to be relatively weak. In this context, it is interesting to note that yet another decay channel from excited ternary Li particles was discussed by Feather [5], who interpreted the observed coincident emission of tritons and α particles [45] to originate from the decay of ^{7}Li when created in its excited state at 4.63 MeV. For the reactions ^{233,235}U($n_{\rm th}$,f), coincident ^{3}H-α emission was recently reexamined in Ref. [46] confirming the occurrence of these rather highly excited ^{7}Li LCPs in TF. Also the appearance of ^{8}Be in short-lived excited states was recently established in TF of ^{233,235}U($n_{\rm th}$,f) [46] and ^{252}Cf(sf) [47], as an admixture to the emission of ^{8}Be in its ground state. Since ^{8}Be is particle-unstable for a decay into two α particles, ternary ^{8}Be from both, the ground and excited state, disintegrate in flight, but at different stages of acceleration and with different Q values. The decay from the different states can thus be distinguished by the mutual α-α angular correlations. Both recent experiments on the subject proved also the occurrence of ''quaternary'' fission where two LCPs (α-α and ^{3}H-α) are emitted apparently independently from each other right at scission.

The possible existence of long-lived complex nuclear molecules in particular ternary scission-point configurations has been hypothesized from investigating the γ decay of ^{10}Be-accompanied ^{252}Cf(sf) [7–11]. It has to be stressed that the neutron decay from excited ternary ^{8}Li* nuclei gives no hint for a comparably large delay in the ^{8}Li* emission. The measured neutron angular distribution tells that the breakup of ^{8}Li*, being faster than the γ decay of ^{10}Be* by seven orders of magnitude, occurs after the LCP is fully accelerated, hence leaving no indication for the formation of a nuclear molecule with lifetime larger than $\sim 10^{-20}$ s (see Fig. 12). However, the formation of nuclear molecules may depend on the LCP structure and/or be more likely for LCPs with nuclear charges $Z > 3$ and masses $A > 8$. Unfortunately the very low yields of these processes make further experiments on the issue rather difficult.

ACKNOWLEDGMENTS

Yu.N.K. wants to thank the DAAD, Bonn for a research grant. The experiment was conducted in collaboration with P. Singer, M. Clemens, A. Hotzel, and M. Hesse, and was supported by the BMBF, Bonn (Contract Nos. 06DA461 and 06TU669). The authors are indebted to N. V. Kornilov for providing the ^{252}Cf neutron data used for calibration purposes, and to S. R. Neumaier for his expertise in performing LCP trajectory and yield calculations.

[1] C. Wagemans, in *Particle Emission from Nuclei*, edited by D. N. Poenaru and M. S. Ivascu (CRC Press, Boca Raton, 1989), Chap. 3.
[2] C. Wagemans, in *The Nuclear Fission Process*, edited by C. Wagemans (CRC Press, Boca Raton, 1991), Chap. 12.
[3] M. Mutterer and J.P. Theobald, in *Nuclear Decay Modes*, edited by D.N. Poenaru (IOP, Bristol, England, 1996), Chap. 12.
[4] F. Gönnenwein, M. Wöstheinrich, M. Hesse, H. Faust, G. Fioni, and S. Oberstedt, in *Proceedings of the Seminar on Fission, Pont d'Oye IV, Habay-la-Neuve, Belgium, 1999*, edited by C. Wagemans, O. Serot, and P. D'hondt (World Scientific, Singapore, 2000), p. 59.
[5] N. Feather, Proc. R. Soc. Edinburgh **71**, 21 (1974).
[6] G. Valskii, Yad. Fiz. **24**, 270 (1976) [Sov. J. Nucl. Phys. **24**, 140 (1976)].
[7] P. Singer, Yu. Kopatch, M. Mutterer, M. Klemens, A. Hotzel, D. Schwalm, P. Thirolf, and M. Hesse, in *Proceedings of the International Conference on Dynamical Aspects of Nuclear Fission, DANF96, Častá Papiernička, Slovakia*, edited by J. Kliman and B. I. Pustylnik (JINR, Dubna, 1996), p. 262; P. Singer, Ph.D. thesis, TU Darmstadt, 1997.
[8] M. Mutterer, P. Singer, M. Klemens, Yu. Kopatch, D. Schwalm, P. Thirolf, A. Hotzel, M. Hesse, and F. Gönnenwein, in *Proceedings of the International Conference on Fission and Properties of Neutron Rich Nuclei, Sanibel Island, Florida*, edited by J. H. Hamilton and A. V. Ramayya (World Scientific, Singapore, 1998), p. 119.
[9] A.V. Ramayya, J.K. Hwang, J.H. Hamilton, A. Sandulescu, A. Florescu, G.M. Ter-Akopian, A.V. Daniels, G.S. Popeko, Yu. Oganessian, W. Greiner, J.D. Cole, and GANDS Collaboration, Phys. Rev. Lett. **81**, 947 (1998).
[10] J.H. Hamilton, A.V. Ramayya, J.K. Hwang, W. Greiner, S.J. Zhu, A. Sandulescu, A. Florescu, J. Kormicki, G.M. Ter-Akopian, Yu. Oganessian, A.V. Daniel, G.S. Popeko, J. Kliman, M. Morháč, J.D. Cole, R. Aryaeinejad, M.W. Drigert, W.E. Collins, W.C. Ma, E.F. Jones, L.K. Peker, P.M. Gore, G. Drafta, B.R.S. Babu, G. Wang, and J.K. Deng, Acta Phys. Slov. **49**, 31 (1999).
[11] W. Greiner, Acta Phys. Slov. **49**, 9 (1999).
[12] V.N. Nefedov, O.I. Ivanov, V.P. Kharin, and A.S. Tishin, Yad. Fiz. **3**, 337 (1966) [Sov. J. Nucl. Phys. **3**, 337 (1966)].
[13] E. Cheifetz, B. Eylon, E. Fraenkel, and A. Gavron, Phys. Rev. Lett. **29**, 805 (1972).
[14] A.P. Graevskii and G.E. Solyakin, Yad. Fiz. **18**, 720 (1974) [Sov. J. Nucl. Phys. **18**, 369 (1974)], and references therein.
[15] W. Loveland, Phys. Rev. C **9**, 395 (1974).
[16] F. Caitucoli, B. Leroux, G. Barreau, N. Carjan, T. Benfoughal, T.P. Doan, F. El Hage, A. Sicre, M. Asghar, P. Perrin, and G. Siegert, Z. Phys. A **298**, 219 (1980).
[17] J.K. Hwang, A.V. Ramayya, J.H. Hamilton, C.J. Beyer, J. Kormicki, X.Q. Zhang, A. Rodin, A. Formichev, J. Kliman, L. Krupa, G.M. Ter Akopian, Yu.Ts. Oganessian, G. Hubarian, D. Seweryniak, C.J. Lister, R.V.F. Janssens, I. Ahmad, M.P. Carpenter, J.P. Greene, T. Lauritsen, I. Wiedenhöver, W.C. Ma, R.B. Piercey, and J.D. Cole, Phys. Rev. C **61**, 047601 (2000).
[18] F. Ajzenberg-Selove, Nucl. Phys. **A490**, 1 (1988).
[19] M. Mutterer, P. Singer, Yu. Kopatch, M. Klemens, A. Hotzel, D. Schwalm, P. Thirolf, and M. Hesse, in *Proceedings of the International Conference on Dynamical Aspects of Nuclear Fission, DANF96, Častá Papiernička, Slovakia*, edited by J. Kliman and B. I. Pustylnik (JINR, Dubna, 1996), p. 250.
[20] V. Metag, D. Habs, K. Helmer, U.v. Helmolt, H.W. Heyng, B. Kolb, D. Pelte, D. Schwalm, W. Hennerici, H.J. Hennrich, G. Himmele, E. Jaeschke, R. Repnow, W. Wahl, R.S. Simon, and R. Albrecht, Lect. Notes Phys. **178**, 163 (1983).
[21] P. Singer, M. Mutterer, Yu.N. Kopatch, M. Klemens, A. Hotzel, D. Schwalm, P. Thirolf, and M. Hesse, Z. Phys. A **359**, 41 (1997).
[22] Yu.N. Kopatch, P. Singer, M. Mutterer, M. Klemens, A. Hotzel, D. Schwalm, P. Thirolf, M. Hesse, and F. Gönnenwein, Phys. Rev. Lett. **82**, 303 (1999).
[23] W. Weiter, Diploma thesis, Universitat Heidelberg, 1981.
[24] A. Hotzel, Diploma thesis, Universitat Heidelberg, 1995.
[25] K. Skarsvåg, Nucl. Phys. **A153**, 82 (1970).
[26] Yu.N. Kopatch, Ph.D. thesis, JINR Dubna, 1999.
[27] N.V. Kornilov (private communication).
[28] M. Mutterer, Yu. N. Kopatch, D. Schwalm, P. Thirolf, and F. Gönnenwein (to be published).
[29] A. Schubert, K. Möller, W. Neubert, W. Pilz, G. Schmidt, M. Adler, and H. Märten, Z. Phys. A **338**, 115 (1991).
[30] P. Heeg, J. Pannicke, M. Mutterer, P. Schall, J.P. Theobald, K. Weingärtner, K.F. Hoffmann, P. Zöller, G. Barreau, B. Leroux, and F. Gönnenwein, Nucl. Instrum. Methods Phys. Res. A **278**, 52 (1989).
[31] W. Baum, Ph.D. thesis, TU Darmstadt, 1992.
[32] Z. Dlouhy, J. Svanda, R. Bayer, and I. Wilhelm, in Proceedings of the International Conference on Fifty Years Research in Nuclear Fission, Berlin, edited by D. Hilscher, H. J. Krappe, and W. von Oertzen, Report No. HMI-B 464, 1989, p. 43.
[33] Ş. Mişicu, A. Sandulescu, and W. Greiner, Phys. Rev. C **61**, 041602(R) (2000).
[34] N. Carjan, J. Phys. (France) **37**, 1279 (1976); S. Oberstedt and N. Carjan, Z. Phys. A **344**, 59 (1992).
[35] R. Schäfer and T. Fliessbach, J. Phys. G **21**, 861 (1995).
[36] V. Grachev, Yu.I. Gusev, and D.M. Seliverstov, Yad. Fiz. **47**, 622 (1988) [Sov. J. Nucl. Phys. **47**, 395 (1988)].
[37] A.A. Vorobyov, D. Seliverstov, V. Grachev, I. Kondurov, A. Nikitin, A. Yegorov, and Y. Zalite, Phys. Lett. **40B**, 102 (1972).
[38] I. Halpern, Annu. Rev. Nucl. Sci. **21**, 245 (1971).
[39] V.A. Rubchenya and S.G. Yavshits, Z. Phys. A **329**, 217 (1988).
[40] A. Pik-Pichak, Phys. At. Nucl. **57**, 906 (1994).
[41] M. Mutterer, Yu. Kopatch, P. Singer, M. Klemens, A. Hotzel, D. Schwalm, P. Thirolf, M. Hesse, and F. Gönnenwein, in *Proceedings of the 2nd International Conference on Fission and Properties of Neutron Rich Nuclei, St. Andrews, Scotland*, edited by J. H. Hamilton, W. R. Phillips, and H. K. Carter (World Scientific, Singapore, 2000), p. 316.
[42] C. Wagemans and O. Serot, in *Proceedings of the 2nd International Conference on Fission and Properties of Neutron Rich Nuclei, St. Andrews, Scotland*, edited by J. H. Hamilton, W. R. Phillips, and H. K. Carter (World Scientific, Singapore, 2000), p. 340.
[43] H. H. Knitter, U. Brosa, and C. Budtz-Jørgensen, in *The Nuclear Fission Process*, edited by C. Wagemans (CRC Press, Boca Raton, 1991), p. 11.
[44] I. Tilquin, Y. El Masri, M. Parlog, Ph. Collon, M. Hadri, Th. Keutgen, J. Lehmann, P. Leleux, P. Lipnik, A. Ninane, F. Hanappe, G. Bizard, D. Durand, P. Mosrin, J. Peter, R. Regim-

bart, and B. Tamin, Nucl. Instrum. Methods Phys. Res. A **365**, 446 (1995).

[45] S. K. Kataria, E. Nardi, and S.G. Thompson, in *Proceedings of the 3rd IAEA Symposium on the Physics and Chemistry of Fission, Rochester, NY* (IAEA, Vienna, 1973), p. 389.

[46] F. Gönnenwein, P. Jesinger, M. Mutterer, A.M. Gagarski, G.A. Petrov, W.H. Trzaska, V. Nesvishevski, and O. Zimmer, in *Proceedings of the International Workshop on Fission Dynamics of Atomic Clusters and Nuclei, Luso, Portugal, 2000*, edited by J. de Providencia (World Scientific, Singapore, in press).

[47] Yu. N. Kopatch, M. Mutterer, J. von Kalben, H.-J. Wollersheim, E. Lubkiewicz, and P. Adrich, GSI Scientific Report 2000, No. GSI-2001-1, 2001, p. 23.